IUBMB *Life*, 59(8–9): 578–585, August–September 2007

informa
healthcare

Critical Review

Cold-Adapted Signal Proteins: NMR Structures of Pheromones from the Antarctic Ciliate *Euplotes nobilii*

William J. Placzek[1,2], Touraj Etezady-Esfarjani[1,*], Torsten Herrmann[1,*], Bill Pedrini[1,2], Wolfgang Peti[1,†], Claudio Alimenti[3], Pierangelo Luporini[3] and Kurt Wüthrich[1,2]

[1]*Department of Molecular Biology, The Scripps Research Institute, La Jolla, California, USA*
[2]*Skaggs Institute for Chemical Biology, The Scripps Research Institute, La Jolla, California, USA*
[3]*Dipartimento di Biologia Molecolare Cellulare e Animale, University of Camerino, Camerino (MC), Italy*

Summary

Cell type-specific signal proteins, known as pheromones, are synthesized by ciliated protozoa in association with their self/nonself mating-type systems, and are utilized to control the vegetative growth and mating stages of their life cycle. In species of the most ubiquitous ciliate, *Euplotes*, these pheromones form families of structurally homologous molecules, which are constitutively secreted into the extracellular environment, from where they can be isolated in sufficient amounts for chemical characterization. This paper describes the NMR structures of E*n*-1 and E*n*-2, which are members of the cold-adapted pheromone family produced by *Euplotes nobilii*, a species inhabiting the freezing coastal waters of Antarctica. The structures were determined with the proteins from the natural source, using homonuclear ^{1}H NMR techniques in combination with automated NOESY peak picking and NOE assignment. E*n*-1 and E*n*-2 have highly homologous global folds, which consist of a central three-α-helix bundle with an up-down-up topology and a 3_{10}-helical turn near the N-terminus. This fold is stabilized by four disulfide bonds and the helices are connected by bulging loops. Apparent structural specificity resides in the variable C-terminal regions of the pheromones. The NMR structures of E*n*-1 and E*n*-2 provide novel insights into the cold-adaptive modifications that distinguish the *E. nobilii* pheromone family from the closely related *E. raikovi* pheromone family isolated from temperate waters.

IUBMB *Life*, 59: 578–585, 2007

Keywords Protein structures; ciliate pheromones; cell recognition signals; disulfide-bond identification; Antarctic biology.

Received 27 December 2006; accepted 29 December 2006

Address correspondence to: Kurt Wüthrich, Department of Molecular Biology, MB-44, The Scripps Research Institute, 10550 North Torrey Pines Rd., La Jolla, CA 92037, USA.
Tel: +1 858 784 8011. Fax: +1 858 784 8014.
E-mail: wuthrich@scripps.edu

Present addresses: *Institut für Molekularbiologie und Biophysik, ETH Zürich, CH-8093 Zürich, Switzerland. †Department of Molecular Pharmacology, Physiology and Biotechnology, Brown University, 70 Ship Street, G-E3, Providence, RI 02912, USA.

ISSN 1521-6543 print/ISSN 1521-6551 online © 2007 IUBMB
DOI: 10.1080/15216540701258165

INTRODUCTION

The exploration of organisms living in extreme environments has shed light on how life spread everywhere liquid water is available on our planet, irrespective of other physical and geochemical conditions (*1*). Even the most hostile and harsh habitats have been found to harbour a great variety of organisms, mostly archea and bacteria, which thrive under environmental extremes and are designated as 'extremophiles'. Among these, psychrophiles and thermophiles, i.e., organisms able to grow at temperatures close to 0°C and up to 80°C, respectively, have generated keen interest for the unique opportunities that they provide to assess relationships between protein stability, dynamics and function, as well as for the economic potential of their proteins for direct industry use or as models for the engineering of mesophilic counterparts (*2, 3*).

While the molecular properties of thermophilic proteins, which are often readily overexpressed, purified and characterized, have been extensively studied (*4–8*), cold-adapted proteins have so far been subject to much more limited research. In view of their extensive distribution and occurrence in the biosphere, much of which is mostly cold, with temperatures permanently below 5°C, much work remains to be done. In recent years, a handful of structures have been determined for enzymes of psychrophilic microorganisms (*9, 10*) and 'anti freeze proteins' (*11–15*), and insights have been obtained from site-directed mutagenesis experiments (*16*) and directed evolution methods (*17*) on the structural principles that govern protein cold-adaptation. To a greater extent than in thermophilic adaptation, the psychrophilic protein families appear to make use of more varied strategies to maintain their functional efficiency in thermodynamically unfavourable environments. Widening of the solvent-accessible areas, weakening of the compactness of the hydrophobic core, or extension of surface loops have most commonly been

proposed to act synergistically or individually to acquire increased backbone flexibility without affecting stability in cold-adapted proteins (*18, 19*).

A new avenue to insights into the structural modifications underlying protein cold-adaptation may be provided by studies of a family of structurally homologous proteins that can be purified in amounts of 50–150 μg of protein/litre of culture supernatant from an eukaryotic antarctic marine eukaryotic microbe, the ciliate *Euplotes nobilii* (*20*). These proteins are collectively designated as 'pheromones' and distinguished from one another by the denominations E*n*-1, E*n*-2, ... They represent cell type-specific environmental signals on which the cells rely to shift between the vegetative (growth) and mating (sexual) stages of their life cycle (*21*). In contrast to the cold-adapted protein families studied so far which are mostly represented by structurally complex enzymes specialized for a specific catalytic activity in the cells (*2, 18*) or by antifreeze proteins (*11–15*), the *E. nobilii* pheromones are small water-borne proteins with hormonal activity. As such, they are likely to be under stronger adaptive pressure to balance their molecular structures between increased flexibility required to bind effectively to their cell receptors, and high stability required for a long-lasting and long-range activity in a permanently freezing environment. Therefore, the adaptive significance of their structural specificities should, at least in principle, be more directly apparent and more readily accessible to experimental analysis. In this paper, we have determined the NMR structures of the two *E. nobilii* pheromones E*n*-1 and E*n*-2. Analysis of these two structures provides initial insights into potentially distinctive structural features of the E*n* pheromone family. Corresponding data on another E*n* pheromone, E*n*-6, are forthcoming (*22*).

MATERIALS AND METHODS

Protein Preparation and NMR Spectroscopy

Isolation and purification of E*n*-1 and E*n*-2 from native cell cultures were performed as previously described (*23*). For both proteins, 1.3 mg were dissolved in a volume of 300 μl to obtain 1 mM protein concentration in 20 mM phosphate buffer at pH 6.0, either in 95% H_2O/5% D_2O, or in 100% D_2O. Shigemi tubes were used for the NMR experiments. Sequence-specific backbone and side chain assignments were obtained using the following homonuclear ^1H experiments with H_2O and D_2O solutions of the pheromones (*24*): 2D [^1H,^1H]-COSY, 2D [^1H,^1H]-TOCSY with a mixing time $\tau_m = 65$ ms, 2D [^1H,^1H]-NOESY with a mixing time $\tau_m = 150$ ms. The spectra were recorded at 303 K on a Bruker Avance600 spectrometer. For the structure determination, two 2D [^1H,^1H]-NOESY spectra were recorded with a mixing time $\tau_m = 85$ ms at 303 K on a Bruker DRX800 spectrometer in protein solutions in 95% H_2O/5% D_2O, and in 100% D_2O, respectively. All NMR spectra were analyzed using the software XEASY (*25*).

Collection of Conformational Constraints and 3D Structure Calculation

The NOESY spectra were analyzed with the automated ATNOS/CANDID approach (*26, 27*) in combination with structure calculation, using the torsion angle molecular dynamics algorithm DYANA (*28*). For each protein, the input for the iterative ATNOS/CANDID procedure consisted of the chemical shift lists obtained from the previous sequence-specific resonance assignment, and of two 2D [^1H,^1H]-NOESY spectra recorded in H_2O and in D_2O solution, respectively. During the first six ATNOS/CANDID cycles, ambiguous distance constraints were used (*29*). For the final structure calculation in cycle 7, only distance constraints were retained that could be unambiguously assigned based on the protein 3D structure resulting from cycle 6. φ and ψ backbone dihedral angle constraints derived from the $^{13}C^{\alpha}$ chemical shifts (*30, 31*), torsion angle constraints derived from the $^1H-^1H$ coupling constants using the grid search procedure FOUND (*32*), and disulfide bond constraints (*33*) were added to the input for each cycle of structure calculation. The disulfide-bonded cysteine pairs were identified by the following procedure (*34*). First, two reference calculations, without disulfide constraints and with ambiguous disulfide constraints (*35*), respectively, were performed. Through the analysis of the distances $d_{\beta\beta}$ between each possible combination of pairs of Cys residues, the correct disulfide pairings were identified. These disulfide bond assignments were verified through the observation of $H^{\beta}-H^{\beta}$ NOEs in the NOESY spectra. The 20 conformers with the lowest residual DYANA target function values obtained from cycle 7 were energy-refined in a water shell with the program OPALp (*36, 37*). The program MOLMOL (*38*) was used to analyze the protein structures and to prepare the figures showing molecular models.

RESULTS

Resonance Assignment, Constraint Collection and Structure Calculation

The sequence-specific resonance assignments of E*n*-1 (52 residues, MW = 5630, Swiss-Prot: P83441) and E*n*-2 (60 residues, MW = 6304, Swiss-Prot: P83235) were conducted using standard homonuclear NMR techniques (*24*). For E*n*-1, all 47 expected backbone amide proton resonances were identified. Nearly complete sequence-specific resonance assignments were obtained, with a single gap between residues Tyr31 and Thr32 (Fig. 1), and all non-labile side-chain protons were assigned for the residues 2–52. Similarly, for E*n*-2 all 56 expected backbone amide proton resonances were identified, and complete sequence-specific resonance assignments were obtained (Fig. 1). For the side-chains, all the non-labile protons were assigned, with the sole exception of Phe40 H^{ζ}. In addition, 25 and 27 $^{13}C^{\alpha}$ chemical shifts were assigned for E*n*-1

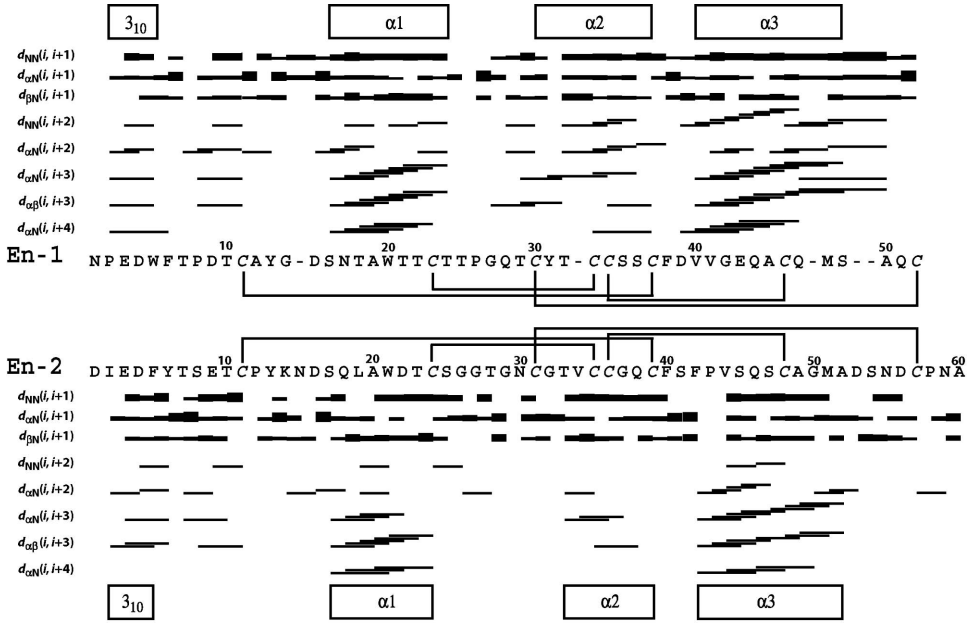

Figure 1. Alignment of the amino acid sequences of E*n*-1 and E*n*-2 based on the CLUSTALW algorithm (*39*) and survey of the sequential and medium-range 1H-1H NOEs observed in E*n*-1 and E*n*-2 (*24*). The disulfide bonds in E*n*-1 and E*n*-2 identified in this paper are indicated. Above the E*n*-1 sequence, the sequential assignments and the collection of medium-range NOE constraints for E*n*-1 are surveyed (not shown are the Xxx-Pro sequential connectivities, which were in all cases established by *d*12 and/or *d*22 NOEs). For the sequential NOEs *d*NN, *d*1N, and *d*4N, the thickness of the bars corresponds to the NOE intensities, and the medium-range NOEs *d*NN(*i,i* + 2), *d*1N(*i,i* + 2), *d*1N(*i,i* + 3), *d*14(*i,i* + 3) and *d*1N(*i,i* + 4) are indicated by lines connecting the two related residues. The locations of regular secondary structures in E*n*-1 are identified at the top. The corresponding information for E*n*-2 is presented below the E*n*-2 sequence.

and E*n*-2, respectively, based on natural abundance 2D [^{13}C,^{1}H]-COSY spectra. For both proteins the side chain –NH_n groups of Asn, Gln and Trp have also been assigned. The chemical shift lists of E*n*-1 and E*n*-2 have been deposited in the BMRB (www.bmrb.wisc.edu) with accession numbers 7326 and 7327, respectively.

The structure calculations of E*n*-1 and E*n*-2 were performed using automated NOESY peak picking and NOE assignment with the routines ATNOS (*26*) and CANDID (*27*) in conjunction with the DYANA (*28*) torsion angle molecular dynamics algorithm, as described in Materials and Methods. The input of conformational constraints was derived from [^{1}H,^{1}H]-NOESY spectra recorded in H_2O- and D_2O-solutions at T = 303 K with a mixing time of 85 ms, and from measurements of $^{3}J_{HN\alpha}$ coupling constants and $^{13}C^{\alpha}$ chemical shifts.

For the final structure calculation of E*n*-1 in cycle 7, a total of 2440 NOE cross peaks were unambiguously assigned, leading to a total of 746 meaningful NOE upper distance limits. In addition, 274 torsion angle constraints were derived with the FOUND grid search algorithm (*32*) from short-range NOEs and 50 $^{3}J_{HN\alpha}$ coupling constants, and from 25 $^{13}C^{\alpha}$ chemical shifts (*30, 31*). The input for DYANA was further supplemented with 32 upper and lower disulfide distance limits (*33, 34*). The 20 conformers with the lowest DYANA target function values were energy-minimized with the program OPALp (*36, 37*) and used to represent the solution structure of E*n*-1 (Fig. 2). The statistics of Table 1 show that a high-quality structure determination was achieved.

For E*n*-2, a total of 3103 NOE cross peaks were unambiguously assigned, leading to a total of 696 meaningful NOE upper distance limits. 277 torsion angle constraints derived from short-range NOEs, 54 $^{3}J_{HN\alpha}$ coupling constants and 27 $^{13}C^{\alpha}$ chemical shifts (*30–32*), as well as 32 upper and lower disulfide bond constraints supplemented the input for the final structure calculation. The 20 energy-minimized conformers with the lowest DYANA target function values representing the solution structure of E*n*-2 (Fig. 3) represent a high-quality structure determination (Table 1).

The NMR Solution Structures of En-1 and En-2

The solution structures of E*n*-1 and E*n*-2 are closely homologous, and therefore they are described jointly in this section. Each protein contains two regular α-helices, α1 and α3, a somewhat distorted α-helix, α2, and a 3_{10}-helical turn

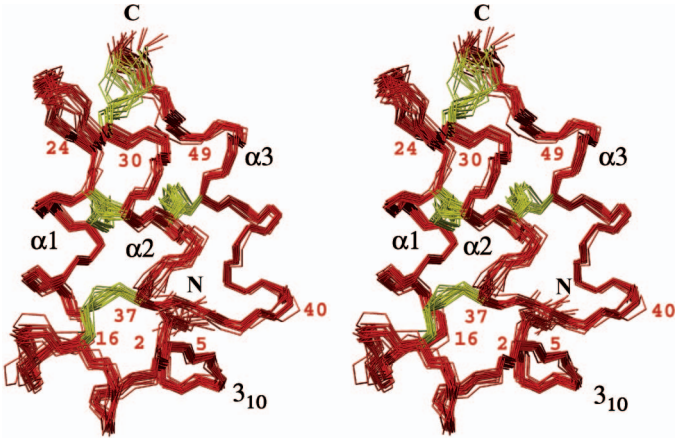

Figure 2. Stereo view of the bundle of 20 energy-minimized DYANA conformers that represent the NMR structure of E*n*-1. The conformers were superimposed for pair-wise minimum RMSD values of the backbone atoms N, C1 and C′ of residues 2–52. The four disulfide bonds are highlighted in gold. The two chain ends are identified by N and C, and the regular secondary structures are identified, with the first and last residue of each helix indicated by red numbers.

(Fig. 4). The two regular α-helices span the residues 16–24 (α1) and 40–49 (α3) in E*n*-1, and 17–24 (α1) and 42–52 (α3) in E*n*-2; the distorted α-helix spans the residues 30–37 in E*n*-1 and 33–39 in E*n*-2; and the 3_{10}-helical turn spans the residues 2–5 in both E*n*-1 and E*n*-2 (Figs 2–4). In E*n*-1, the cysteine pairs 11–37, 23–33, 34–46 and 30–52 form four disulfide bonds, and in E*n*-2 the equivalent cysteine pairs 11–39, 24–35, 36–48 and 31–57 are formed (Fig. 1). Two disulfide bonds link the helices α1 and α3 to α2, one bond links the N-terminal loop with the C-terminal end of the helix α2, and the fourth disulfide bond connects the loop following α1 to a position at or near the C-terminus (Fig. 1). The three core helices α1, α2 and α3 of E*n*-1 and E*n*-2 are organized in an up-down-up arrangement that forms a trigonal pyramid, with the C-terminus located at the top of the pyramid (Figs 2–4). In E*n*-1, the helix α2 is anti-parallel to α1 (Fig. 2), while in E*n*-2 the helix α2 is anti-parallel with α3 (Fig. 3). The 3_{10}-helical turn of residues 2–5 and the loop 6–16 are located at the base of the pyramid formed by the three core helices and close off the hydrophobic core of the protein.

DISCUSSION

Common Structural Features of En Family Pheromones

With the determination of the structures of two *E. nobilii* pheromones, we are able to identify an apparent blueprint of their molecular architectures, since the secondary and tertiary structures of E*n*-1 and E*n*-2 exhibit extensive similarities. The alignment of their sequences with the ClustalW algorithm (*39*) required the insertion of five gaps in the sequence of E*n*-1 in order to bring the eight cysteines into register (Fig. 1). Once brought into register, the cysteine residues form four corresponding disulfide bonds, which are located in nearly identical positions in the three-dimensional structures of E*n*-1 and E*n*-2, although the polypeptide segments leading from the helix α3 to the last cysteinyl residue is elongated by two residues in E*n*-2 when compared to E*n*-1. The two proteins also contain similar sets of four helical secondary structures, with three antiparallel helices α1, α2 and α3 organized in a trigonal pyramidal fashion (Fig. 4). The two molecules also share the following two traits: Firstly, two disulfide bonds link the helices α1 and α3 to α2. Secondly, the 3_{10}-helical turn near the N-terminus and the well-structured loop connecting this turn with α1 form a base of the pyramid formed by the three core helices.

Structural Specificities of Individual En Pheromones

With the core scaffold being largely conserved in E*n*-1 and E*n*-2, two local structural variations are readily apparent. First, the distorted helix α2 is shortened by one residue in E*n*-2 (Fig. 4), which results in an elongation of the flexible loop following helix α1. Apparently as a result of these sequence and secondary structure variations, the axis of helix α2 runs parallel to the axis of α1 in E*n*-2 (Fig. 4), while the axis of the helix α2 of E*n*-1 runs parallel to the axis of α3 (Fig. 4). Secondly, the two proteins show variable lengths of the helices α3, and the sequence of E*n*-2 is elongated beyond the last Cys residue by a tripeptide segment. These two variable regions form a contiguous surface area of the pheromones.

Variation of the structures near the C-terminal chain end was previously proposed as a structural basis for pheromone-specificity, based on the results of a study of *E. raikovi* pheromones (*40*). Additional support for this hypothesis now comes from the three E*n* structures presented here, since structural differences between these three proteins near their C-termini and in the loop region following the helix α1 represent a structurally and electrostatically variable site, which accommodates nearly all the insertions in E*n*-2 when compared to E*n*-1.

The aforementioned variations of sequence and conformation lead to pronouncedly different charge distributions on the surface near the C-terminus (Fig. 5). E*n*-1 has a large cleft of negatively charged surface extending from the base of the trigonal pyramid formed by the core helices toward the top of the pyramid, whereby the two proteins show clearly different patterns of charge distribution, due to the fact that the shorter C-terminus of E*n*-1 creates a flat C-terminal surface that is devoid of surface-accessible negative charges (Fig. 5). These pronounced variations of surface charge distribution are highly likely to ensure specificity for the interactions with the pheromone receptors, as has also been suggested for the pheromone–receptor interactions in *E. raikovi,* based on the

Table 1
Input for the structure calculation in ATNOS/CANDID cycle 7 and characterization of the bundles of 20 energy-minimized DYANA conformers that represent the NMR structures of E*n*-1 and E*n*-2

Parameter	E*n*-1[a]	E*n*-2[a]
NOE upper distance limits	746	696
Intraresidual	119	168
Short-range	222	211
Medium-range	222	127
Long-range	183	190
Dihedral angle constraints	274	277
Disulfide bond constraints	32	32
Residual target function values (Å^2)	0.71 ± 0.17	0.94 ± 0.19
Residual NOE violations		
Number ≥ 0.1 Å	7 ± 2 (3–11)	8 ± 2 (4–13)
Maximum (Å)	0.12 ± 0.01 (0.11–0.13)	0.12 ± 0.01 (0.11–0.14)
Residual dihedral angle violations		
Number ≥ 2.5 deg	2 ± 1 (0–3)	1 ± 1 (0–2)
Maximum (deg)	5.66 ± 3.79 (2.37–13.37)	4.06 ± 2.76 (1.88–10.92)
AMBER energies (kcal/mol)		
Total	-1723.13 ± 48.82	-1854.80 ± 39.69
van der Waals	-137.71 ± 7.39	-143.42 ± 7.76
Electrostatics	-1951.83 ± 45.69	-2148.44 ± 33.44
rmsd from ideal geometry		
Bond lengths (Å)	0.0073 ± 0.0002	0.0080 ± 0.0006
Bond angles (deg)	1.86 ± 0.06	2.01 ± 0.18
rmsd to the mean coordinates (Å)[b]		
bb (3–50/3–57)	0.36 ± 0.05 (0.29–0.43)	0.39 ± 0.08 (0.25–0.51)
ha (3–50/3–57)	0.73 ± 0.05 (0.65–0.81)	0.75 ± 0.05 (0.67–0.84)
Ramachandran plot statistics (%)[c]		
Most favored regions	73.6	71.1
Additional allowed regions	22.2	25.9
Generally allowed regions	1.9	1.6
Disallowed regions	2.3	1.4

[a]Except for the top two entries, the average value for the 20 energy-minimized conformers with the lowest residual DYANA target function values and the standard deviation among them are given, with minimum and maximum values given in parentheses.
[b]bb indicates the backbone atoms N, C^{α}, C′; ha stands for 'all heavy atoms'. The numbers in parentheses indicate the residues for which the rmsd was calculated.
[c]As determined by PROCHECK (*50*).

intermolecular contacts in the crystal structure of the pheromone E*r*-1 (*41*).

Molecular Structures and Cold Adaptation

The N-terminal polypeptide segments preceding the helix α1 of the pheromones E*n*-1 and E*n*-2 are a well-structured entity that caps off the hydrophobic core created by the three α-helices (Fig. 6). No corresponding, well-structured N-terminal region has been found in any of the *E. raikovi* pheromone structures (*42–48*). In both E*n* pheromones the N-terminal surface exhibits similar sets of exposed negatively charged side-chains, including the conserved and homologous residues Glu 3, Asp/Glu 4 and Asp/Glu 8/9 (Fig. 6). Similar orientation of these side-chains (Fig. 6) ensures that the base of both pheromone structures is dominated by negative charges (Fig. 5).

Overall, it thus appears that the N-terminus represents a molecular region where the pressure for cold adaptation has restricted the divergence in the pheromone sequences, whereas in the loop following α1 and near the C-terminus, cold

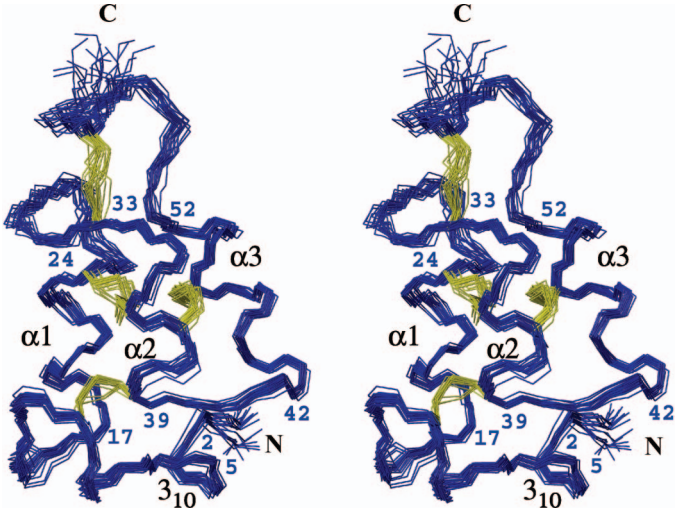

Figure 3. Stereo view of the bundle of 20 energy-minimized DYANA conformers that represent the NMR structure of E*n*-2. Same presentation as in Fig. 2, with the 20 conformers superimposed for pair-wise minimum RMSD values of the backbone atoms N, C1 and C′ of residues 2–58.

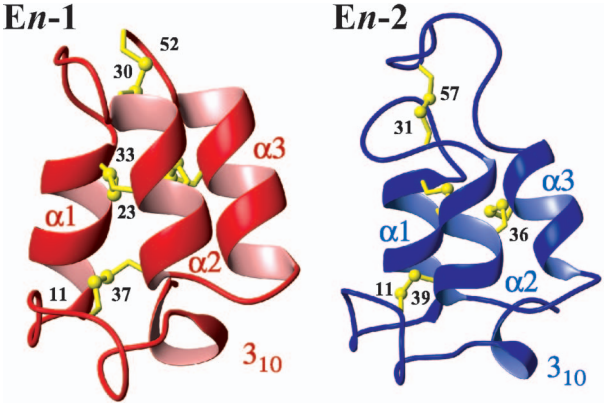

Figure 4. Ribbon presentations of the structures of E*n*-1 and E*n*-2, showing the DYANA conformer with the lowest backbone RMSD to the mean atom coordinates. The helical secondary structures α1, α2 and α3, and a 3_{10}-helical turn are identified. The sequence locations of the eight cysteinyl residues are also indicated. 637 × 942 mm (72 × 72 DPI).

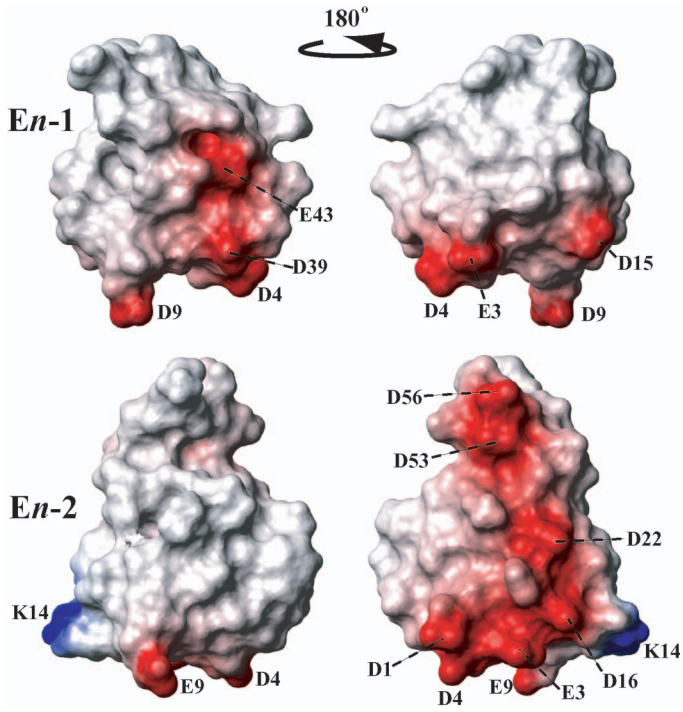

Figure 5. Front and back views of the surface electrostatic potential distributions of E*n*-1 and E*n*-2. Red and blue color indicates negatively and positively charged surface areas, respectively. In each pheromone, the residues responsible for the electrostatic surface charges are labeled. The orientation on the left corresponds to the viewing angle of the structures in Fig. 4. 681 × 1128 mm (72 × 72 DPI).

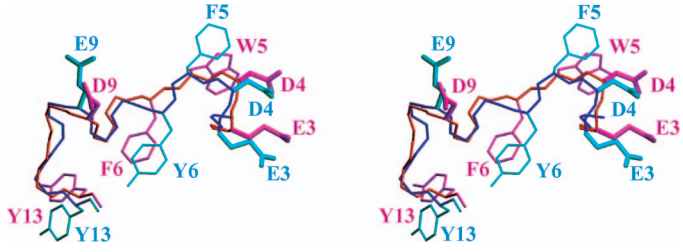

Figure 6. Stereo view of a comparison of the polypeptide segments 3–13 of E*n*-1 (backbone red, side chains magenta) and E*n*-2 (backbone dark blue, side chains cyan). The superposition is for minimal RMSD calculated for the backbone heavy atoms of residues 3–13. The negatively charged side chains and the aromatic side chains are shown and identified (see text). 621 × 747 mm (72 × 72 DPI).

adaptation has been combined with a large degree of sequence variation between the two pheromones in order to retain functional specificity. In both of these molecular regions, incorporation of glycine, threonine and serine residues appears to maintain the flexibility of the interaction surface in the extreme cold environment of *E. nobilii* that is needed for successful pheromone receptor binding (*19, 49*).

ACKNOWLEDGEMENTS

Financial support: Skaggs Institute for Chemical Biology, fellowships for WJP and BP; Swiss National Science Foundation, stipends for TEE and TH through project 31-66427.01 to KW, and fellowship PA00A-109047/1 to BP; Italian PNRA support for the PL and CA laboratory. KW is the Cecil H. and

Ida M. Green Professor of Structural Biology and a member of the Skaggs Institute for Chemical Biology at The Scripps Research Institute. The use of the high-performance computing facilities of The Scripps Research Institute is gratefully acknowledged.

REFERENCES

1. Rothschild, L. J., and Mancinelli, R. L. (2001) Life in extreme environments. *Nature* **409**, 1092–1101.
2. Feller, G., and Gerday, C. (2003) Psychrophilic enzymes: hot topics in cold adaptation. *Nat. Rev. Microbiol.* **1**, 200–208.
3. Gerday, C., Aittaleb, M., Bentahir, M., Chessa, J. P., Claverie, P., Collins, T., D'Amico, S., Dumont, J., Garsoux, G., Georlette, D., Hoyoux, A., Lonhienne, T., Meuwis, M. A., and Feller, G. (2000) Cold-adapted enzymes: From fundamentals to biotechnology. *Trends Biotechnol.* **18**, 103–107.
4. Criswell, A. R., Bae, E., Stec, B., Konisky, J., and Phillips, G. N., Jr. (2003) Structures of thermophilic and mesophilic adenylate kinases from the genus *Methanococcus*. *J. Mol. Biol.* **330**, 1087–1099.
5. Perl, D., Mueller, U., Heinemann, U., and Schmid, F. X. (2000) Two exposed amino acid residues confer thermostability on a cold shock protein. *Nat. Struct. Biol.* **7**, 380–383.
6. Lesley, S. A., Kuhn, P., Godzik, A., Deacon, A. M., Mathews, I., Kreusch, A., Spraggon, G., Klock, H. E., McMullan, D., Shin, T., Vincent, J., Robb, A., Brinen, L. S., Miller, M. D., McPhillips, T. M., Miller, M. A., Scheibe, D., Canaves, J. M., Guda, C., Jaroszewski, L., Selby, T. L., Elsliger, M. A., Wooley, J., Taylor, S. S., Hodgson, K. O., Wilson, I. A., Schultz, P. G., and Stevens, R. C. (2002) Structural genomics of the *Thermotoga maritima* proteome implemented in a high-throughput structure determination pipeline. *Proc. Natl. Acad. Sci. USA* **99**, 11664–11669.
7. Peti, W., Etezady-Esfarjani, T., Herrmann, T., Klock, H. E., Lesley, S. A., and Wüthrich, K. (2004) NMR for structural proteomics of *Thermotoga maritima*: Screening and structure determination. *J. Struct. Funct. Genomics* **5**, 205–215.
8. Robinson-Rechavi, M., and Godzik, A. (2005) Structural genomics of *Thermotoga maritima* proteins shows that contact order is a major determinant of protein thermostability. *Structure* **13**, 857–860.
9. Arnorsdottir, J., Kristjansson, M. M., and Ficner, R. (2005) Crystal structure of a subtilisin-like serine proteinase from a psychrotrophic vibrio species reveals structural aspects of cold adaptation. *FEBS J.* **272**, 832–845.
10. Bae, E., and Phillips, G. N., Jr. (2004) Structures and analysis of highly homologous psychrophilic, mesophilic, and thermophilic adenylate kinases. *J. Biol. Chem.* **279**, 28202–28208.
11. Davies, P. L., and Sykes, B. D. (1997) Antifreeze proteins. *Curr. Opin. Struct. Biol.* **7**, 828–834.
12. Gronwald, W., Loewen, M. C., Lix, B., Daugulis, A. J., Sonnichsen, F. D., Davies, P. L., and Sykes, B. D. (1998) The solution structure of type II antifreeze protein reveals a new member of the lectin family. *Biochemistry* **37**, 4712–4721.
13. Liou, Y. C., Daley, M. E., Graham, L. A., Kay, C. M., Walker, V. K., Sykes, B. D., and Davies, P. L. (2000) Folding and structural characterization of highly disulfide-bonded beetle antifreeze protein produced in bacteria. *Protein Expr. Purif.* **19**, 148–157.
14. Sonnichsen, F. D., Davies, P. L., and Sykes, B. D. (1998) NMR structural studies on antifreeze proteins. *Biochem. Cell Biol.* **76**, 284–293.
15. Graether, S. P., Slupsky, C. M., and Sykes, B. D. (2006) Effect of a mutation on the structure and dynamics of an alpha-helical antifreeze protein in water and ice. *Proteins* **63**, 603–610.
16. D'Amico, S., Gerday, C., and Feller, G. (2001) Structural determinants of cold adaptation and stability in a large protein. *J. Biol. Chem.* **276**, 25791–25796.
17. Miyazaki, K., Wintrode, P. L., Grayling, R. A., Rubingh, D. N., and Arnold, F. H. (2000) Directed evolution study of temperature adaptation in a psychrophilic enzyme. *J. Mol. Biol.* **297**, 1015–1026.
18. Cavicchioli, R. (2006) Cold-adapted archaea. *Nat. Rev. Microbiol.* **4**, 331–343.
19. Olufsen, M., Smalas, A. O., Moe, E., and Brandsdal, B. O. (2005) Increased flexibility as a strategy for cold adaptation: a comparative molecular dynamics study of cold- and warm-active uracil DNA glycosylase. *J. Biol. Chem.* **280**, 18042–18048.
20. Alimenti, C., Ortenzi, C., Carratore, V., and Luporini, P. (2003) Cold-adapted *Euplotes* pheromones. *Eur. J. Protistol.* **39**, 399–403.
21. Luporini, P., Alimenti, C., Ortenzi, C., and Vallesi, A. (2005) Ciliate mating types and their specific protein pheromones. *Acta Protozoologica* **44**, 89–101.
22. Pedrini, B., Placzek, W. J., Koculi, E., Alimenti, C., LaTerza, A., Luporini, P., and Wüthrich, K. (2007) Cold-adaptation in sea-water-borne signal proteins: Sequence and NMR structure of the pheromone E*n*-6 from the antarctic ciliate *Euplotes nobilii*. Submitted.
23. Felici, A., Alimenti, C., Ortenzi, C., and Luporini, P. (1999) Purification and initial characterization of two pheromones from the marine antarctic ciliate, *Euplotes nobilii*. *Ital. J. Zool.* **66**, 355–360.
24. Wüthrich, K. (1986) *NMR of Proteins and Nucleic Acids*, Wiley, New York.
25. Bartels, C., Xia, T. H., Billeter, M., Güntert, P., and Wüthrich, K. (1995) The program XEASY for computer-supported NMR spectral-analysis of biological macromolecules. *J. Biomol. NMR* **6**, 1–10.
26. Herrmann, T., Güntert, P., and Wüthrich, K. (2002) Protein NMR structure determination with automated NOE-identification in the NOESY spectra using the new software ATNOS. *J. Biomol. NMR* **24**, 171–189.
27. Herrmann, T., Güntert, P., and Wüthrich, K. (2002) Protein NMR structure determination with automated NOE assignment using the new software CANDID and the torsion angle dynamics algorithm DYANA. *J. Mol. Biol.* **319**, 209–227.
28. Güntert, P., Mumenthaler, C., and Wüthrich, K. (1997) Torsion angle dynamics for NMR structure calculation with the new program DYANA. *J. Mol. Biol.* **273**, 283–298.
29. Nilges, M., Macias, M. J., O'Donoghue, S. I., and Oschkinat, H. (1997) Automated NOESY Iinterpretation with ambiguous distance restraints: the refined NMR solution structure of the pleckstrin homology domain from beta-spectrin. *J. Mol. Biol.* **269**, 408–422.
30. Spera, S., and Bax, A. (1991) Empirical correlation between protein backbone conformation and C^{α} and C^{β} ^{13}C nuclear-magnetic-resonance chemical-shifts. *JACS* **113**, 5490–5492.
31. Luginbühl, P., Szyperski, T., and Wüthrich, K. (1995) Statistical basis for the sse of $^{13}C^{\alpha}$ chemical-shifts in protein-structure determination. *J. Mag. Reson.* **B 109**, 229–233.
32. Güntert, P., Billeter, M., Ohlenschläger, O., Brown, L. R., and Wüthrich, K. (1998) Conformational analysis of protein and nucleic acid fragments with the new grid search algorithm FOUND. *J. Biomol. NMR* **12**, 543–548.
33. Williamson, M. P., Havel, T. F., and Wüthrich, K. (1985) Solution conformation of proteinase inhibitor IIA from bull seminal plasma by 1H nuclear magnetic resonance and distance geometry. *J. Mol. Biol.* **182**, 295–315.
34. Fadel, V., Bettendorff, P., Herrmann, T., de Azevedo, W. F., Jr., Oliveira, E. B., Yamane, T., and Wüthrich, K. (2005) Automated NMR structure determination and disulfide bond identification of the myotoxin crotamine from *Crotalus durissus terrificus*. *Toxicon* **46**, 759–767.

35. Nilges, M. (1995) Calculation of protein structures with ambiguous distance restraints. Automated assignment of ambiguous NOE crosspeaks and disulphide connectivities. *J. Mol. Biol.* **245**, 645–660.
36. Luginbühl, P., Güntert, P., Billeter, M., and Wüthrich, K. (1996) The new program OPAL for molecular dynamics simulations and energy refinements of biological macromolecules. *J. Biomol. NMR* **8**, 136–146.
37. Koradi, R., Billeter, M., and Güntert, P. (2000) Point-centered domain decomposition for parallel molecular dynamics simulation. *Comput. Phys. Commun.* **124**, 139–147.
38. Koradi, R., Billeter, M., and Wüthrich, K. (1996) MOLMOL: A program for display and analysis of macromolecular structures. *J. Mol. Graph* **14**, 51–55, 29–32.
39. Thompson, J. D., Higgins, D. G., and Gibson, T. J. (1994) CLUSTALW: Improving the sensitivity of progressive multiple sequence alignment through sequence weighting, position-specific gap penalties and weight matrix choice. *Nucleic Acids Res.* **22**, 4673–4680.
40. Luginbühl, P., Ottiger, M., Mronga, S., and Wüthrich, K. (1994) Structure comparison of the pheromones E*r*-1, E*r*-10, and E*r*-2 from *Euplotes raikovi*. *Protein Sci.* **3**, 1537–1546.
41. Weiss, M. S., Anderson, D. H., Raffioni, S., Bradshaw, R. A., Ortenzi, C., Luporini, P., and Eisenberg, D. (1995) A cooperative model for receptor recognition and cell adhesion: Evidence from the molecular packing in the 1.6-Å crystal structure of the pheromone E*r*-1 from the ciliated protozoan *Euplotes raikovi*. *Proc. Natl. Acad. Sci. USA* **92**, 10172–10176.
42. Brown, L. R., Mronga, S., Bradshaw, R. A., Ortenzi, C., Luporini, P., and Wüthrich, K. (1993) Nuclear magnetic resonance solution structure of the pheromone E*r*-10 from the ciliated protozoan *Euplotes raikovi*. *J. Mol. Biol.* **231**, 800–816.
43. Di Giusepp, G., Miceli, C., Zahn, R., Damberger, F., Wüthrich, K., and Luporini, P. (2002) A structurally deviant member of the *Euplotes raikovi* pheromone family: E*r*-23. *J. Eukaryot. Microbiol.* **49**, 86–92.
44. Liu, A., Luginbühl, P., Zerbe, O., Ortenzi, C., Luporini, P., and Wüthrich, K. (2001) NMR structure of the pheromone E*r*-22 from *Euplotes raikovi*. *J. Biomol. NMR* **19**, 75–78.
45. Luginbühl, P., Wu, J., Zerbe, O., Ortenzi, C., Luporini, P., and Wüthrich, K. (1996) The NMR solution structure of the pheromone E*r*-11 from the ciliated protozoan *Euplotes raikovi*. *Protein Sci.* **5**, 1512–1522.
46. Mronga, S., Luginbühl, P., Brown, L. R., Ortenzi, C., Luporini, P., Bradshaw, R. A., and Wüthrich, K. (1994) The NMR solution structure of the pheromone E*r*-1 from the ciliated protozoan *Euplotes raikovi*. *Protein Sci.* **3**, 1527–1536.
47. Ottiger, M., Szyperski, T., Luginbühl, P., Ortenzi, C., Luporini, P., Bradshaw, R. A., and Wüthrich, K. (1994) The NMR solution structure of the pheromone E*r*-2 from the ciliated protozoan *Euplotes raikovi*. *Protein Sci.* **3**, 1515–1526.
48. Zahn, R., Damberger, F., Ortenzi, C., Luporini, P., and Wüthrich, K. (2001) NMR structure of the *Euplotes raikovi* pheromone E*r*-23 and identification of its five disulfide bonds. *J. Mol. Biol.* **313**, 923–931.
49. Siddiqui, K. S., and Cavicchioli, R. (2006) Cold-adapted enzymes. *Annu. Rev. Biochem.* **75**, 403–433.
50. Morris, A. L., Macarthur, M. W., Hutchinson, E. G., and Thornton, J. M. (1992) Stereochemical quality of protein-structure coordinates. *Proteins* **12**, 345–364.